Specific Interaction and Two-Dimensional Crystallization of Histidine Tagged Yeast RNA Polymerase I on Nickel-Chelating Lipids

Nicolas Bischler,* Fabrice Balavoine,# Philipp Milkereit,§ Herbert Tschochner,§ Charles Mioskowski,# and Patrick Schultz*

*Institut de Génétique et de Biologie Moléculaire et Cellulaire, CNRS/INSERM/ULP 1, F-67404 Illkirch Cedex, C.U. de Strasbourg, Strasbourg, France; #Service des molécules marquées, DBCM, CEA, Centre d'Etudes de Saclay, F-91191 Gif-sur-Yvette Cedex, France; and §Biochemie Zentrum (BZH), Universität Heidelberg, D-69120 Heidelberg, Germany

ABSTRACT Nickel-chelating lipid monolayers were used to generate two-dimensional crystals from yeast RNA polymerase I that was histidine-tagged on one of its subunits. The interaction of the enzyme with the spread lipid layers was found to be imidazole dependent, and the formation of two-dimensional crystals required small amounts of imidazole, probably to select the specific interaction of the engineered tag with the nickel. Two distinct preparations of RNA polymerase I tagged on different subunits yielded two different crystal forms, indicating that the position of the tag determines the crystallization process. The orientation of the enzyme in both crystal forms is correlated with the location of the tagged subunits in a three-dimensional model which shows that the tagged subunits are in contact with the lipid layer.

INTRODUCTION

Complex biological systems integrate multiple interdependent functions located on large macromolecular assemblies. The biological activity relies on interactions with additional polypeptides or ligands, and the functional tuning generally involves the specific binding of regulatory proteins. To understand the mechanism of action of such arrangements, biochemical and genetic information has to be correlated with structural data on the complexes in various functional states.

Electron microscopy is widely used for the structural study of such macromolecular complexes, because unlike x-ray crystallography or NMR, this method is not limited by the size of the particle. Structural information over a wide range of resolution can be recorded, from the size of the particle down to 0.3 to 0.4 nm. The contrast of unstained biological samples is low, and the preservation of small structural details requires low electron doses to reduce irradiation damage. These two main reasons impair the signal-to-noise ratio of the electron micrographs and hinder their direct visual interpretation. The aim of computerized image analysis is to average a large number of molecular images to improve the signal-to-noise ratio and to statistically validate high-resolution structural features. The attainable resolution by image analysis is determined by the capacity to define the direction along which the specimen is observed and the relative azimuthal angles of the molecules. Self-assembly of biological macromolecules into regular arrays is thus a prerequisite for high-resolution structural studies by electron microscopy, because the molecules are uniquely oriented. Helical symmetry (Unwin, 1993), but most efficiently two-dimensional (2-D) crystals revealed the structure of membrane proteins at almost atomic resolution (Henderson et al., 1990; Kühlbrandt et al., 1994).

Originally restricted to membrane proteins that are naturally inserted or interacting with lipid bilayers, methods were developed to study soluble proteins. Amphiphilic molecules form self-assembled structures when they are spread at the surface of a buffered solution and provide unique properties usable for orienting and organizing biological macromolecules (Uzgiris and Kornberg, 1983; Lebeau et al., 1996). The biophysical properties of lipid layers, such as fluidity and stability, have proved to be essential to promoting the self-organization of proteins on a surface (Lebeau et al., 1996). A major task was to attract the macromolecules close to the lipid layer spread on a Langmuir trough. For this purpose, two types of interactions were used that mimic the binding used in ion-exchange and affinity chromatography, respectively. Nonspecific electrostatic interactions can be formed between charged lipid layers and discrete domains at the surface of protein molecules (Darst et al., 1989). This approach proved to be successful for both single polypeptides (Celia et al., 1996; Ellis et al., 1997) or large molecular assemblies such as DNA-dependent RNA polymerases from different organisms (Darst et al., 1989; Edwards et al., 1994; Schultz et al., 1990) or 50S ribosomal subunits (Avila-Sakar et al., 1994). Specific interactions between the macromolecule of interest and the lipid layer can be promoted by derivatizing the hydrophilic part of the lipid molecule with a ligand of the biomolecule of interest (Uzgiris and Kornberg, 1983; Ribi et al., 1987; Darst et al., 1991a; Lebeau et al., 1990). This latter method has several advantages contributed by the specificity of the interaction. The environment of the macromolecules tethered to the lipid interface can be better controlled, and the face of the protein inter-

Received for publication 5 September 1997 and in final form 18 November 1997.

Address reprint requests to Dr. Patrick Schultz, Institut de Génétique et de Biologie Moléculaire et Cellulaire, CNRS/INSERM/ULP 1, rue Laurent Fries, BP163, F-67404 Illkirch Cedex, C.U. de Strasbourg, France. Tel.: 33-3-88-65-53-85; Fax: 33-3-88-65-53-05; E-mail: pat@wotan.u-strasbg.fr.

0006-3495/98/03/1522/11 $2.00

acting with the film can be predicted. Finally, the purity requirements for the protein are less stringent, because it could be demonstrated in several instances that the addition of a contaminant protein to the macromolecule of interest does not perturb the crystallization process (Lebeau et al., 1990; Mosser and Brisson, 1991). The drawback of such an approach is a time-consuming chemical and pharmacological study of the binding characteristics of partially derivatized, soluble ligands to determine the possible anchor sites of the ligand on the lipid moiety. Moreover, because each ligand binding site is different, accessibility requirements have to be fulfilled, which implies the synthesis of a battery of compounds differing by the length of a linking arm between the ligand and the lipid (Lebeau et al., 1990).

There is therefore a general demand for a more universal lipid support that would allow the 2-D crystallization of virtually any protein or macromolecular complex. As a step in this direction, we describe here the use of nickel-chelating lipids to crystallize proteins genetically modified by a hexahistidine tag (His_6 tag). These interactions are widely used in immobilized metal ion affinity chromatography for the purification of proteins or peptides (Porath et al., 1975). The metal-chelating nitriloacetic acid (NTA) group (Hochuli et al., 1987) was linked to a lipid molecule to allow the coordination of histidine residues accessible on the protein.

Yeast RNA polymerase I was used in this study because it is a sound example of a large molecular complex containing more than 10 different subunits with a total molecular mass higher than 600 kDa. There are few high-affinity ligands for RNA polymerases, and it is therefore a challenging task to genetically modify the enzyme to introduce a specific interaction with the metal-chelating lipid. A His_6 tag was therefore introduced into the coding sequence of one of the subunits, which, once expressed in a suitable yeast strain, is incorporated into the complex to form an active enzyme. Yeast RNA polymerase I was previously crystallized in two dimensions by using positively charged lipid layers (Schultz et al., 1990), which provides the unique opportunity to compare the properties of both types of crystallization procedures based on a nonspecific and a specific interaction, respectively. A three-dimensional model of the solvent-accessible surface of this enzyme is available (Schultz et al., 1993) that will be useful to determine which face of the enzyme contacts the lipid film. Moreover, the His_6-tagged subunits were located on the enzyme surface by immuno-electron microscopy (Klinger et al., 1996; Lanzendörfer et al., 1997) and thus will allow us to control whether the tagged subunit is indeed in contact with the lipid film. The results show that under well-defined imidazole concentrations, the chelating lipids can be used to crystallize a large macromolecular complex tagged on one of its subunits. The use of two preparations of RNA polymerase tagged on two distinct subunits clearly demonstrates that the engineered His_6 tag mediates the enzyme-lipid interaction leading to crystallization.

MATERIALS AND METHODS

Lipid synthesis

Specific lipids

The synthesis is based on a convergent approach proceeding through the preparation of a nickel-chelating nitrilotriacetic group and 2-(1,3-di-*O*-oleyl-glyceroxy)-acetic acid, which are coupled to lead to the desired functionalized lipid, 2-(bis-carboxymethyl-amino)-6-[2-(1,3-di-*O*-oleyl-glyceroxy)-acetyl-amino] hexanoic acid (NTA-DOGA). The NTA group was elaborated from Z-N_6-L-lysine as previously described by Hochuli et al. (1987). A complete esterification of this triacid derivative was performed in methanol with a few drops of sulfuric acid. For the lipid skeleton synthesis, the glycerol moiety was obtained in a one-step procedure by reacting epibromhydrin with 2 equivalents of oleyl alcohol in the presence of NaH, affording the symmetrical dialkylglycerol ether (Altenburger et al., 1992). Acetylation of the 1,3-di-*O*-oleyl-glycerol with *tert*-butyl bromoacetate followed by an hydrolysis led to the corresponding acid. The coupling reaction between 2-(1,3-di-*O*-oleyl-glyceroxy)-acetic acid and the methyl nitrilotriacetate derivative was performed in dichloromethane in the presence of dicyclohexylcarbodiimide and 4-dimethylaminopyridine to give the expected functionalized lipid, the trimethylester of NTA-DOGA. The latter was reduced in methanol to the corresponding distearyl derivative (trimethylester of NTA-DSA) by catalytic hydrogenation, using palladium on activated carbon (10%). Trimethylesters of NTA-DOGA and NTA-DSA were quantitatively hydrolyzed in a mixture of ethylene glycol dimethylether and water by the addition of an aqueous potassium hydroxide solution to yield the triacids of NTA-DOGA and NTA-DSA, respectively. For complexing Ni^{2+} ions, a chloroform solution of lipid was stirred with an aqueous buffer (pH 8) containing one equivalent of $NiCl_2 \cdot 6H_2O$. After 30 min, we observed the blue-green coloration of the organic phase. The organic phase was concentrated under vacuum to obtain the corresponding nickel-chelating lipid Ni-NTA-DOGA (or Ni-NTA-DSA), which was used without further purification. The structure and purity of NTA-DOGA and NTA-DSA were assessed and confirmed by UV, IR, proton, and ^{13}C NMR spectroscopy and mass spectrometry (Balavoine et al., manuscript in preparation). Final products are shown in Fig. 1.

Nonspecific lipids

L-α-Phosphatidylcholine from fresh egg yolk, stearylamine, L-α-phosphatidylserine from bovine brain, oleyl alcohol, and dioleyl trimethyl ammonium were from Sigma-Aldrich Chemical Company (St. Louis, MO).

Yeast strains

Yeast strain LS 149 (kindly provided by A. Sentenac and his colleagues) contained a His_6-tagged AC_{40} subunit (MATα ade2 ura3 trp1 his3 lys2

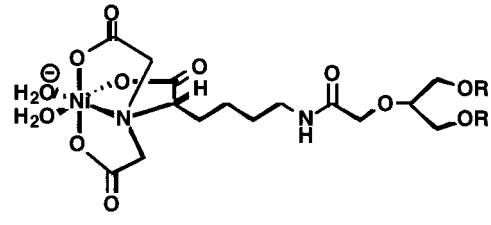

Ni-NTA-DOGA : R = Oleyl = $(CH_2)_8CH{=}CH(CH_2)_7CH_3$

Ni-NTA-DSA : R = Stearyl = $(CH_2)_{17}CH_3$

FIGURE 1 Structure of the functionalized Ni^{2+}-chelating lipids: 2-(bis-carboxymethyl-amino)-6-[2-(1, 3-di-O-oleyl-glyceroxy)-acetyl-amino] hexanoic acid (Ni-NTA-DOGA) and 2-(bis-carboxymethyl-amino)-6-[2-(1, 3-di-O-stearyl-glyceroxy)-acetyl-amino] hexanoic acid (Ni-NTA-DSA).

rpc40::His3 with plasmid pLS200 URA3, CEN, HA-RPC40−6histidine), and strain YF2089 (kind gift of D. Friesen and colleagues) was His tagged at subunit ABC23 (MATα ade2 ura3 trp1 his3 leu2 rpb6:: LEU2 with plasmid pFL39 TRP1, CEN/ARS RPB6−6Histidine). (The subunit nomenclature identifies the yeast enzyme class to which it belongs (A (I), B (II), and C (III)) and the apparent size of the polypeptide in kDa $\times 10^{-3}$.)

RNA polymerase purification

Yeast RNA polymerase I was purified as described by Milkereit et al. (manuscript submitted for publication). Briefly, yeast whole cell extract was chromatographed on a DEAE Sepharose column. The RNA polymerase I-containing fractions were identified and quantified by Western blot analysis with antibodies directed against the RNA polymerase I-specific subunit A_{49} (kindly provided by A. Sentenac and colleagues) and by the RNA polymerase-dependent ability to synthesize RNA in a nonspecific manner from single-stranded DNA templates.

The 350 mM potassium chloride eluate of the DEAE Sepharose column contained the RNA polymerase I activity and was extensively dialyzed against low salt containing buffer. The precipitate, which was dissolved in a buffer containing 600 mM potassium acetate, was shown to contain most of the total RNA polymerase I activity and was virtually devoid of RNA polymerase II and III, as was determined by Western blot analysis.

This fraction was further chromatographed on a BioRex 70 column, and the RNA polymerase I-specific activity was eluted in a single step with 2 M potassium acetate. Gel filtration of this fraction on Sephacryl S-300 in a buffer containing 600 mM potassium acetate revealed a rather broad distribution of RNA polymerase I through the column. The largest detectable RNA polymerase I-containing complexes migrated at a position corresponding to a molecular mass of more than 10^6 Da and contained a large proportion of the dimeric form of the enzyme, as evidenced by direct electron microscopy observation of the fraction. Three 1.5-ml fractions were stored at −80°C at a final protein concentration of 50−100 μg/ml in buffer A (20 mM HEPES, pH 7.8, 600 mM potassium acetate, 2 mM $MgCl_2$, 0.02 mM EDTA, 20% glycerol).

Untagged yeast RNA polymerase I (a kind gift from A. Sentenac and colleagues) was purified and assayed as previously described (Huet et al., 1982).

Specimen preparation

To study the interaction and crystallization of His_6-tagged RNA polymerases with the specific lipids, 10 μl of buffer B (20 mM Tris, pH 7.5, 5 mM $MgCl_2$, 20% glycerol) was placed in a Teflon well 4 mm in diameter and 1 mm deep. The surface of the droplet was coated with 0.5–1 μl of Ni-NTA-DOGA or Ni-NTA-DSA lipids at a concentration of 0.5 mg/ml in chloroform/hexane (1:1, v/v). Five microliters of the RNA polymerase I suspension at a concentration of 100 μg/ml was injected into the subphase to reach a final potassium acetate concentration of 200 mM. The preparation was allowed to incubate for times ranging between 30 min and 48 h at 4°C or at 18°C in a humid chamber. Thereafter, a 300-mesh copper/rhodium electron microscopy grid, covered with a freshly evaporated 10-nm-thick carbon film, was placed on top of the well with the carbon film contacting the droplet. The grid was withdrawn after 2 min of adsorption, rinsed with double-distilled water, and negatively stained for 30 s with a 2% uranyl acetate solution. The quality of the transfer was found to be affected by the side of the grid on which the carbon foil was deposited. Schmutz and Brisson (1996) showed that the metal surface roughness is different for the rhodium side as compared to the copper side, and that the rougher the surface, the flatter the carbon foil. We found similarly that the number of transferred crystals was correlated with the use of a flat carbon foil, although the quality (e.g., the degree of order) of the crystals was not affected.

Electron microscopy and image processing

Micrographs were recorded on Kodak SO163 films at a magnification of 45,000×, using a Phillips CM120 transmission electron microscope operating at 100 kV and at minimal electron dose conditions (<10 electrons/Å^2). Electron micrographs were checked by optical diffraction for the absence of astigmatism and for optimal contrast transfer function. The best micrographs were printed and digitized on a flatbed scanner (Powerlook II, UMAX) at 42 μm raster size, corresponding to 0.5 nm on the specimen.

Image analysis was performed with the IMAGIC statistical module (Van Heel and Keegstra, 1981). Briefly, crystal images were processed to normalize the variance of the pixel density and to set the average pixel density to zero. This image was multiplied by a smooth-edged circular mask with a diameter 0.9 times the diameter of the image, to minimize the influence of the mask on the shape of the peaks in the Fourier transform. Fourier transforms were calculated for these masked areas and displayed as power spectra. Strong peaks were interactively selected and were used to find additional peaks and to refine the reciprocal lattice. Amplitude and phases of the peaks having amplitudes at least 1.5 times above background and falling on the reciprocal lattice were selected from the Fourier transform. A filtered image was then calculated by back-Fourier transforming the masked peaks. The filtered image was centered on a putative twofold symmetry by translational alignment of its 180°-rotated transform. The central 128 × 128 pixel area of the centered filtered image was used as cross-correlation reference as described by Saxton (1980). The individual unit cells whose coordinates are determined from the position of peaks in the cross-correlation function are extracted from the original image and averaged to produce a noise-free image. The structure factors of the image are extracted from the Fourier transform of the average image to determine the extent of symmetry and the resolution.

RESULTS

His_6-tagged RNA polymerase binds to Ni-NTA-DOGA lipids through metal chelation

The purified RNA polymerase I containing a His_6-tagged subunit AC_{40} was incubated at a final concentration of 30 μg/ml with the Ni-NTA-DOGA lipid spread on the air/buffer interface. A large number of RNA polymerase molecules were transferred to the electron microscopy grid. Most of the enzyme molecules were aggregated into filament-like structures, and no crystalline area could be observed (Fig. 2 *A*).

To demonstrate that the binding of the enzyme to the Ni-NTA-DOGA lipid was mediated by a chelating interaction, increasing amounts of imidazole were added to the incubation buffer. Imidazole serves as an electron donor competing with the protein for the coordination of nickel. At a final concentration of 40 mM and up to 90 mM imidazole, oval-shaped ordered areas 0.3–2 μm in size were observed (Fig. 2 *B* and Table 1). These crystalline areas were often arranged along strings connected by protein filaments. A high concentration of crystals was thus observed locally, separated by large areas devoid of any bound protein. RNA polymerase molecules were found to bind to the lipid layer up to an imidazole concentration of 200 mM, whereas at higher concentrations of competitor the enzyme no longer bound. These observations indicated that an excess of imidazole prevented the interaction of RNA polymerase with the Ni-NTA-DOGA lipid layers, but that a minimum imidazole concentration was required to form crystalline areas.

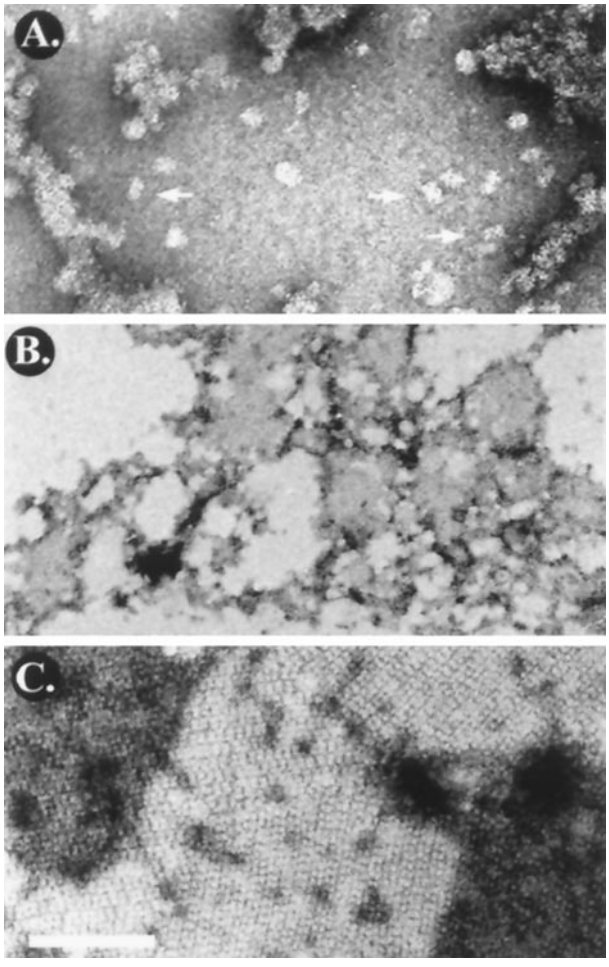

FIGURE 2 Low-magnification electron micrographs showing a Ni-NTA-DOGA film incubated with yeast RNA polymerase I His_6-tagged on subunit AC_{40} at a concentration of 30 μg/ml. (*A*) In the absence of imidazole, most of the transferred enzyme molecules are aggregated. The arrows indicate isolated dimers of RNA polymerase. (*B*) In the presence of 40 mM imidazole and after 1 h of incubation time, dark, oval-shaped domains connected by filamentous structures are observed. These domains contain RNA polymerase molecules arranged in two-dimensional crystals, as shown in Fig. 2 C. (*C*) For incubation times of 24 h, multilayered structures are often observed as domains of higher density. The staining of the different layers was not uniform, so that their exact register could not be determined. The bar represents 100 nm in *A*, 520 nm in *B*, and 200 nm in *C*.

Under these conditions, the formation of crystals was highly reproducible, because 80–90% of all experiments showed crystalline regions. Crystallization was not observed at an ionic strength higher than 200 mM potassium acetate, and the binding of the enzyme to the Ni-NTA-DOGA lipid could be detected up to an ionic strength of 300 mM potassium acetate (Table 1).

The largest crystalline areas were observed after 2 h of incubation at 4°C. Increasing incubation time resulted in a lower number of transferred crystals, in a smaller average size, and in the accumulation of small vesicles on the crystal surface. Incubation times of 24 h or more promoted the formation of multilayered areas identified as dark, oval-shaped domains superposed on existing crystals and consisting of up to four layers (Fig. 2 *C*). In their vast majority the additional layers were smaller than the underlying domain and did not extend beyond its border, suggesting that the second layer was not deposited by chance on the first one. The poor staining of the additional layers did not allow us to determine whether they were organized and were in a unique register with the underlying crystal. If the latter were the case, a moiré pattern would occasionally appear because of slight shifts or rotations between the successive layers. Such patterns were never observed.

To obtain an average view of the crystallized RNA polymerase molecule, five negatively stained crystals such as those shown in Fig. 3 *A*, each containing ~300 unit cells, were analyzed as described in Materials and Methods. The correlation averages of all crystals analyzed were similar (Fig. 3 *B*), and their diffraction pattern could be indexed on an oblique lattice corresponding to a unit cell of $a = 22.6 \pm 0.9$ nm, $b = 12.9 \pm 0.3$ nm, and $\gamma = 110.2° \pm 1.7°$ (Fig. 3 *C*). The refinement of the phase origin of the diffraction peaks identified a twofold axis perpendicular to the crystal plane. Diffraction peaks out to a resolution of 1/2.0 nm^{-1} were consistent with p2 symmetry, showing a phase residual on refinement of less than 25°. An average image was calculated, including 51 reflections out to a resolution of 1/25 nm^{-1}, which corresponded to a data completion of 76% and a mean phase residual of 8.7° (Fig. 3 *D*). The unit cell was composed of a single RNA polymerase dimer observed down its internal twofold axis. As a consequence, the same surface in both RNA polymerase molecules was in contact with the lipid film. The RNA polymerase monomer view was composed of two stain-excluding domains separated by a solvent-accessible groove. The smallest domain corresponded to the position of a previously described thumb-shaped protrusion on the 3-D model of the enzyme (Schultz et al., 1993). The twofold symmetry of the dimer and the asymmetry of the monomer projection unambiguously define the orientation of the enzyme relative to the lipid film. The groove pointed toward the solvent, whereas the apical region of the enzyme contacted the lipid film.

To demonstrate the requirement of the specific lipid, control experiments were performed using charged lipid layers in the same buffer conditions. When L-α-phosphatidylserine, a negatively charged lipid that mimics the charges present on the Ni-NTA-DOGA lipid, was used, the enzyme was found to interact with the film, but no crystalline areas were detected. Weak binding was also observed when L-α-phosphatidylcholine or oleyl alcohol was spread at the air-buffer interface, but crystals did not form. Curiously, little binding was observed with positively charged lipids such as stearylamine or dioleyl trimethyl ammonium. This family of lipids was previously shown to promote the crystallization of RNA polymerases of different origins (Darst et al., 1989, 1991b; Schultz et al., 1990). This discrepancy could be explained by the higher ionic strength used in our experiments (200 mM potassium acetate), which was not suitable for crystallization on charged lipid layers (Table 1).

TABLE 1 Summary of the tested incubation conditions

Crystallization conditions	Observed crystals	Comments
Lipid: Ni-NTA-DOGA	p2 crystals	Largest crystals after 2 h incubation
[Imidazole] = 40–90 mM	a = 22.6 nm, b = 12.9 nm $\gamma = 110.2°$	Multilayers after 24 h
Lipid: Ni-NTA-DOGA [imidazole] = 0 mM	None	Aggregation
Lipid: Ni-NTA-DOGA [imidazole] > 200 mM	None	No binding
Lipid: Ni-NTA-DOGA $[CH_3COOK]$ > 200 mM	None	Binding
Lipid: PS	None	
Lipid: PC or OA	None	Weak binding
Lipid: SA or DOTMA	None	Weak binding
Lipid: Ni-NTA-DOGA [EDTA] > 10 mM	None	Crystals if [EDTA] $\leq$ $[Mg^{2+}]$
Lipid: Ni-NTA-DOGA $[NiSO_4]$ or $[NiCl_2]$ = 5 mM	$p22_12_1$ a = 25.3 nm, b = 25 nm $\gamma = 90°$	
Lipid: Ni-NTA-DSA	None	Binding

Abbreviations: PS, phosphatidylserine; PC, phosphatidylcholine; OA, oleyl alcohol, SA, stearylamine; DOTMA, dioleyl-trimethylammonium; Ni-NTA-DOGA, dioleyl nickel-chelating lipid; Ni-NTA-DSA, distearyl nickel-chelating lipid; brackets, concentration of the substance.

The hypothesis of a chelating interaction was further challenged by adding EDTA to the incubation buffer. A concentration above 10 mM was found to prevent crystal formation, probably by chelating the metal more efficiently than the histidines (Table 1). The addition of divalent or trivalent cations at a final concentration of 5 mM had different effects, depending on the nature of the ion; little transfer of enzyme molecules was observed in the presence of Fe^{3+}, Zn^{2+}, or Cu^{2+}, whereas crystals could be observed in the presence of Ca^{2+} and Mg^{2+}. Although all multivalent cations should be able to out-compete the Ni^{2+} ions chelated by the lipid, this distinct behavior probably reflects the variable affinity of the divalent cations for the NTA moiety and the hexahistidine tag.

Interestingly, a different crystal form was observed in the presence of 5 mM nickel sulfate or nickel chloride (Fig. 4 *A* and Table 1). These crystals still required 50 mM imidazole to grow and did not grow in the presence of 5 mM magnesium sulfate. The diffraction patterns of these crystals were similar and could be indexed on a square lattice of unit cell: $a = 25.3 \pm 0.5$ nm, $b = 25.0 \pm 0.3$ nm, and $\gamma = 90.3° \pm 0.5°$. The refinement of the phase origin of the diffraction peaks identified a twofold axis perpendicular to the crystal plane. Moreover, the characteristic phase relationship $F(h, k) = (-1)^{h+k} F(h, -k)$ was observed for most reflections and indicated the presence, in the crystal plane, of 180° screw axes parallel to the a and b directions. This peculiar symmetry was already suggested by the absence or weakness of odd reflections on the crystallographic axes. The 2-D crystals therefore corresponded to the space group $p22_12_1$. Diffraction peaks out to a resolution of 1/4.0 mn^{-1} were consistent with these symmetries, and an average image including 74 reflections with a mean phase residual of 10.7° was calculated (Fig. 4 *B*). The average unit cell was composed of two RNA polymerase dimers interacting through two opposite faces with the lipid film, which was in apparent contradiction with the assumption that only the tagged subunit should contact the specific lipid. Close inspection of the staining intensity within the unit cell revealed that the pseudo-mirror symmetry-related RNA polymerase dimers were differently stained, suggesting that their environments were different, e.g., that they were at different distances from the lipid layer.

When the nickel sulfate concentration was lowered to 1 mM, this crystalline arrangement coexisted on the same grid square, with the previously described crystals formed in the absence of nickel in solution. At nickel sulfate concentrations higher than 10 mM, no crystals formed, which is in keeping with a competition of the soluble Ni^{2+} and the immobilized Ni^{2+} for the binding of the hexahistidine tag.

The RNA polymerase–Ni-NTA-DOGA interaction involves the polyhistidine tag

We investigated whether the His_6 tag mediated the interaction of the enzyme with the lipid interface, because it has been shown in the case of streptavidine that surface histidines may promote the interaction of the protein with metal-chelating lipids (Pack et al., 1997). To check whether streptavidine could compete with RNA polymerase for binding to the lipid layer, the two proteins were mixed in the crystallization buffer and incubated with the specific lipid. Despite a fivefold molar excess of streptavidine, only the RNA polymerase was recruited to the lipid surface and was still able to crystallize in the above-described buffer conditions.

A wild-type, untagged RNA polymerase preparation was set to crystallize in the same conditions. Little binding and no regular arrangements were observed, suggesting that the presence of a His_6 tag was essential for lipid binding and crystallization. As this latter result could be due to a different purification procedure, an additional control was per-

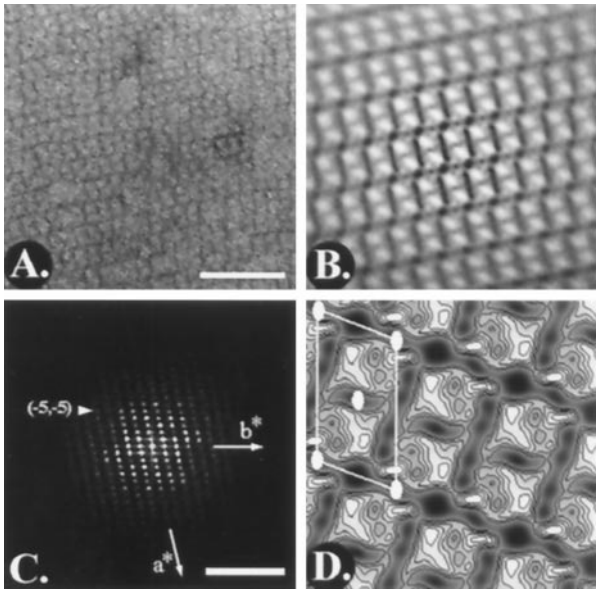

FIGURE 3 Analysis of 2-D crystals of RNA polymerase I molecules His_6-tagged on subunit AC_{40} formed on Ni-NTA-DOGA layers. (*A*) Field of an electron micrograph showing a crystalline area negatively stained with uranyl acetate. The crystal consists of a single molecular layer. The bar represents 80 nm. (*B*) Correlation average image of the crystal shown in *A*. Three hundred subimages were extracted from the crystalline area around coordinates determined from the maxima of the autocorrelation function of the crystal. The image is enlarged twice as compared to *A*. (*C*) Computed power spectrum of the Fourier transformed correlation average shown in *B*. Peaks up to 1/2.6 nm^{-1} are resolved in this pattern (reflection $(-5, -5)$ is marked by an *arrowhead*). The bar represents 0.5 nm^{-1}. (*D*) Two-dimensional projection map, synthesized using 51 terms up to 1/2.6 nm^{-1}. Stain-excluding domains are shown in white and are contoured by lines of equal density. The unit cell is delineated by solid lines, and the twofold axes are shown by small ovals. The unit cell contains two RNA polymerase molecules related by a twofold symmetry. The parameters of the unit cell are $a = 22.6$ nm, $b = 12.9$ nm, and $\gamma = 110.2°$.

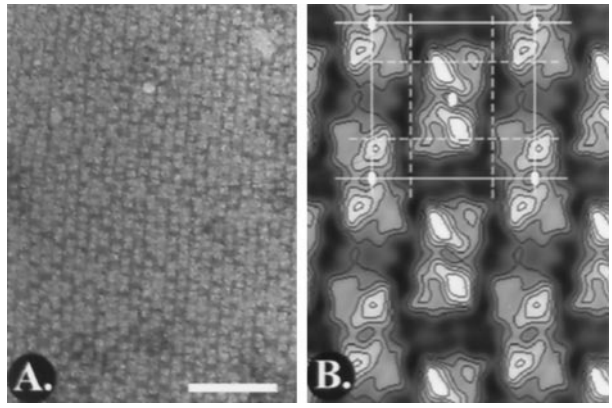

FIGURE 4 Analysis of 2-D crystals of RNA polymerase I molecules His_6-tagged on subunit AC_{40} formed on Ni-NTA-DOGA layers in the presence of 5 mM nickel chloride. (*A*) Field of an electron micrograph showing a crystalline area negatively stained with uranyl acetate. The crystal consists of a single molecular layer. The bar represents 100 nm. (*B*) Two-dimensional projection map synthesized using 74 terms up to 1/4 nm^{-1}. The parameters of the unit cell are $a = 25.3$ nm, $b = 25.0$ nm, and $\gamma = 90.3°$. The unit cell is delineated by solid lines; the twofold axes perpendicular to the crystal plane are shown by small ovals; and the in-plane screw axes are shown by dashed lines. The unit cell contains two RNA polymerase dimers related by a pseudo-mirror symmetry, indicating that the dimers are in reversed orientation. The mirror symmetry is only partially respected, because the staining of dimers in the "up" position is slightly different from that in the "down" position.

formed using a different yeast strain to purify RNA polymerase molecules His_6 tagged on subunit ABC_{23}. Under the same experimental conditions (in particular, 40 mM imidazole), 2-D crystalline regions were obtained (Fig. 5 *A*). The correlation averages of four analyzed crystals were similar, and their diffraction patterns were indexed on an oblique lattice corresponding to a unit cell of $a = 24.0 \pm 0.5$ nm, $b = 13.6 \pm 0.4$ nm, and $\gamma = 99.0° \pm 3°$. A twofold axis perpendicular to the crystal plane was identified upon refinement of the phase origin of the diffraction peaks. Diffraction peaks out to a resolution of 1/4.5 nm^{-1} were consistent with p2 symmetry, and an average image including 29 reflections with a mean phase residual of 6.8° was calculated (Fig. 5 *B*).

The average view of the RNA polymerase molecule as well as the crystal packing were similar to those found in the crystals formed with the AC_{40}-tagged enzyme. The major difference was in that the unit cell of the AC_{40}-tagged enzyme showed a pseudo-mirror symmetry with the AC_{23}-tagged enzyme, indicating that the enzyme interacted with the lipid film in reversed orientation. In contrast to the crystals of the AC_{40}-tagged enzyme grown in the presence of Nickel sulfate and similar to those formed in the absence of nickel sulfate, the orientation of the ABC_{23}-tagged enzyme relative to the lipid film is unique. These data demonstrate that the three-dimensional position of the His_6 tag

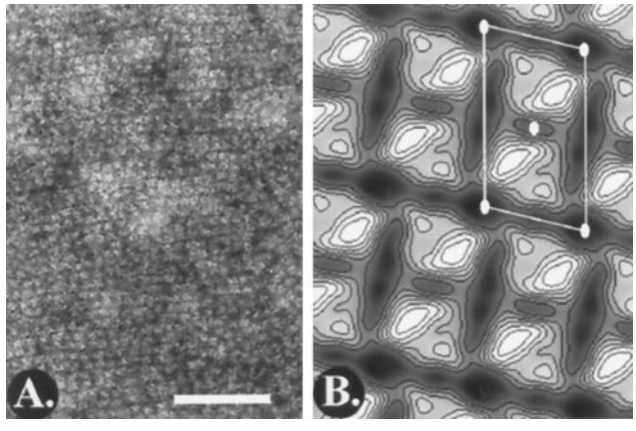

FIGURE 5 Analysis of 2-D crystals of RNA polymerase I molecules His_6-tagged on subunit ABC_{23} formed on Ni-NTA-DOGA layers. (*A*) Field of an electron micrograph showing a crystalline area negatively stained with uranyl acetate. The bar represents 100 nm. (*B*) Two-dimensional projection map synthesized using 29 terms up to 1/4.5 nm^{-1}. The parameters of the unit cell are $a = 24.0$ nm, $b = 13.6$ nm, and $\gamma = 99.0°$. The unit cell is delineated by solid lines; the twofold axes perpendicular to the crystal plane are shown by small ovals. The unit cell contains one RNA polymerase dimer interacting with the lipid layer in the reverse orientation, as compared to the crystals formed when subunit AC_{40} is tagged.

determines the orientation of the enzyme molecules within the crystals formed on Ni-NTA-DOGA lipid layers.

Fluidity of the lipid layers

The in-plane fluidity of the lipid layers was reduced by saturating on the nonpolar oleyl moiety of the lipid molecule to produce stearyl chains. Monolayer compression curves showed that at room temperature, the saturated lipid (Ni-NTA-DSA) was in a crystalline phase, whereas the unsaturated Ni-NTA-DOGA was in a fluid phase (data not shown). When the AC_{40}-tagged RNA polymerase preparation at a final concentration of 20 μg/ml was incubated with Ni-NTA-DSA, the characteristic 2-D crystals did not form (Table 1). Curiously, the grid did not show a uniform distribution of isolated RNA polymerase molecules but, in contrast, was covered with oval-shaped domains similar to those observed when crystallization occurred in the presence of the fluid lipid (Fig. 6 *A*). Within these domains isolated monomeric as well as dimeric forms of the enzyme were observed with a high density and with a stochastic distribution, suggesting that once the RNA polymerase molecule interacts with the lipid film, it is prevented from lateral movement (Fig. 6 *B*). The enzyme preparation could be diluted to a final concentration of 6 μg/ml, and a good coverage of the transferred lipid film was still observed (Fig. 6 *C*). The amount of bound polymerase was roughly proportional to the enzyme concentration. The decrease in protein concentration did not affect the amount of oval-shaped domains transferred onto the grid. These domains were not formed by flattened vesicles, because such structures would show sharp boundaries at their borders, which was not observed.

So far it was difficult to obtain a uniform distribution of well-separated molecules, because fluid lipids promote their interactions. Such a distribution is a prerequisite for structural studies of isolated particles by electron microscopy, allowing us, among other applications, to determine whether the macromolecules of interest are oriented. Visual inspection of the lipid-bound particles indicated that a significant proportion of RNA polymerase dimers was oriented in such a way that the internal p2 axis lay in the plane of the lipid layer. This orientation was in contradiction to the orientation of His_6-tagged RNA polymerase molecules within the crystals, where the internal p2 axis was perpendicular to the lipid plane. Moreover, additional characteristic orientations of the enzyme were detected within the image population. These observations suggested that the RNA polymerase molecules were not specifically and uniquely oriented.

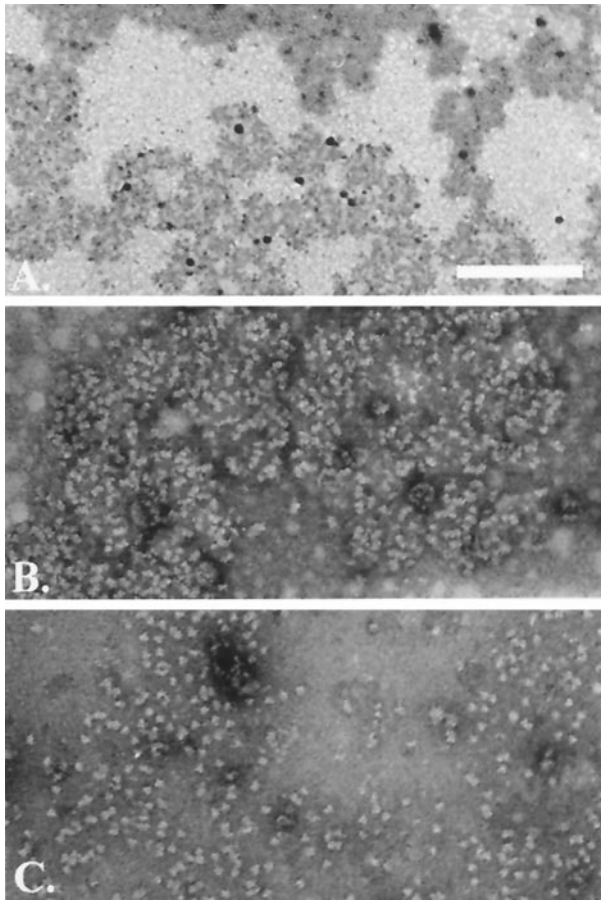

FIGURE 6 Interaction of AC_{40}-tagged RNA polymerase molecules with the saturated Ni-NTA-DSA lipid layer. (*A*) Low-magnification electron micrographs showing oval-shaped dark domains covered with RNA polymerase molecules. Between these domains large areas are devoid of any enzyme molecule. (*B*) When observed at higher magnification, monomeric and dimeric enzyme molecules are clearly observed. At a final RNA polymerase concentration of 20 μg/ml, the macromolecules are closely packed within the domains (~900 molecules/μm^2). Note that the boundaries of the domains are not detectable, indicating that the oval-shaped domains do not correspond to flattened vesicles. (*C*) At a RNA polymerase concentration of 6 μg/ml, the molecular density is lower (~350 molecules/μm^2), but the enzymes are still segregated in oval-shaped domains whose boundaries are not delineated. The bar represents 1 μm in *A* and 290 nm in *B* and *C*.

DISCUSSION

We evaluated the use of a functionalized lipid molecule for its capacity to establish chelator interactions with genetically engineered histidine tags. For this purpose we designed a lipid molecule combining the nickel-chelating nitriloacetic acid (Hochuli et al., 1987) with dioleyl or distearyl glycerol derivatives. A similar approach was successfully used to study the interaction of histidine-containing peptides or proteins with spread monolayers (Schmitt et al., 1994; Dietrich et al., 1995, 1996; Frey et al., 1996; Pack et al., 1997). In these studies, 2-D crystallization of the histidine-tagged proteins was evidenced indirectly by fluorescence microscopy. Two-dimensional crystallization of hexahistidine-tagged proteins by the use of similar lipids was demonstrated at the molecular level by electron microscopy for HIV-1 reverse transcriptase (Kubalek et al., 1994) and for retrovirus core proteins (Barklis et al., 1997). Undoubtedly, a large number of biological systems will benefit

from this method for structural studies, because it can potentially be used for any histidine-tagged protein. Our results characterize the interaction of two genetically modified RNA polymerase with these nickel-chelating lipids and show for the first time the possibility of crystallizing large molecular complexes composed of more than 10 different subunits in which only one component is tagged. Moreover, we show that different crystal groups can be obtained by introducing the tag at a different position on the molecular envelope. This aspect may be of importance for 3-D data collection, because distinct crystals with different molecular orientations will provide the missing information induced by a limited tilt angle. Ultimately it might be possible to orient at will the molecular complexes that could be of importance, to decorate either crystals or isolated molecules with a specific ligand or to study functional variants of the complexes.

Characterization of the protein-lipid interaction

The experiments show that the interaction tethering the polymerase to the lipid monolayer is a chelating interaction. Excess of imidazole, a competitor of the putative specific interaction, prevents the binding and crystallization of the enzyme. A low concentration of imidazole is required for the enzyme to crystallize on these lipids, which reflects the behavior of histidine-tagged proteins in immobilized metal ion affinity chromatography. Small amounts of imidazole are believed to prevent nonspecific binding (mediated, for instance, by surface histidines) and favor the specific interaction with the engineered His_6 tag. We suppose, similarly, that in the absence of imidazole, the RNA polymerase can contact the lipid film through specific and nonspecific interactions. In this case the macromolecules may adopt various orientations with respect to the plane of the lipid layer, thus preventing the establishment of ordered interactions. The frequent observation of protein aggregates in the absence of imidazole suggests that a single RNA polymerase molecule could establish multiple contacts with the lipid layer, thus provoking a wrapping of the film. Crystallization inhibition by high concentrations of divalent cations and by EDTA, which are able to detach the chelated nickel atoms from the lipid, further argues in favor of a coordination interaction involving the nickel atoms. Finally, the absence of crystallization observed when we use nonspecific lipids, either positively charged, negatively charged, or neutral, excludes a major role for electrostatic interactions in the recognition process. This is further emphasized by the absence of effect on the binding of RNA polymerase to the Ni-chelating lipids with the increase of ionic strength to 300 mM potassium acetate.

The interactions leading to crystallization do not necessarily involve the His_6 tag, which might be buried or be weakly accessible compared to a single constitutive histidine exposed at the surface. In this respect it was shown that two surface histidines were responsible for the recognition of streptavidin by copper-chelating lipids (Pack et al., 1997). Although RNA polymerase crystals did not form with the untagged protein, it can be argued that this negative result is due to a different enzyme preparation and a different purification protocol. A more direct demonstration that the engineered His_6 tag influenced the crystallization process was obtained by showing that, when the tag was placed either on subunit AC_{40} or on subunit ABC_{23}, two distinct crystal forms grew that differed by the orientation of the enzyme relatively to the lipid film. The symmetry operators of the crystals indicated that in both arrangements, the same surface of each monomer was in contact with the lipid. In any other orientation of the dimer, such as those found in crystals formed on charged lipids, the two monomers would not contribute equally to the lipid interaction. The structural knowledge of the three-dimensional envelope of the enzyme (Schultz et al., 1993) and the precise location of both subunits within this envelope can be exploited to demonstrate that the modified subunit is in close proximity to the lipid film. Previous immuno-electron microscopy experiments located the tagged subunits on the surface of a three-dimensional model of the enzyme (Klinger et al., 1996; Lanzendörfer et al., 1997). These experiments, summarized in Fig. 7, showed that subunits AC_{40} and ABC_{23} are placed on two opposite faces on the enzyme. This spatial location gives a hint of the reversed orientation of the enzyme in the two crystal forms. Moreover, the three-dimensional model can be oriented relative to the lipid film, as predicted by the location of the subunits, and the model can be used in the same way as an electron microscope to reproject the protein density. The calculated view of the enzyme in both orientations is consistent with the experimental data, thus demonstrating that the tagged subunit is in contact with the lipid film for each RNA polymerase preparation (Fig. 7).

Puzzling results were obtained in the presence of weak concentrations of Ni^{2+} salts. A crystal form in which both "up" and "down" orientations of the RNA polymerase coexist was obtained. This is in contradiction to the conclusion that the orientation of the dimer is determined by the position of the His_6 tag. We propose that the soluble Ni^{2+} ions partially compete with the Ni-chelating lipid for the binding of the His_6 tag and that only a fraction of the RNA polymerase molecules bind to the lipid film. The second orientation of the enzyme molecule would be dictated by protein-protein interactions and would not involve enzyme-lipid interactions. This latter hypothesis is sustained by the observation that the dimers in reversed orientation are not in the same plane, because their staining is slightly different. Similar in-plane screw axes were previously reported in the case of 2-D RNA polymerase crystals formed on charged lipid layers (Schultz et al., 1990; Darst et al., 1991b).

Comparison of specific versus nonspecific interactions

The yeast RNA polymerase I was crystallized in two dimensions through nonspecific electrostatic interactions

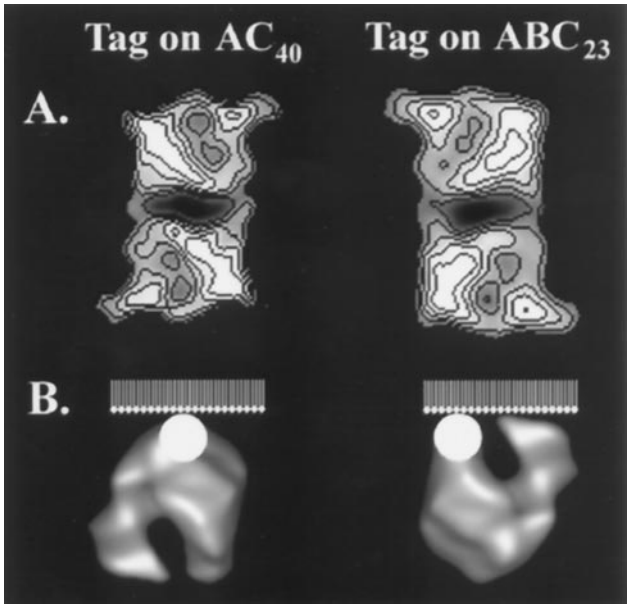

FIGURE 7 Schematic representation of the orientation of the His_6-tagged RNA polymerase molecule upon interaction with the nickel-chelating lipid. (*A*) Two-dimensional projection maps of the crystalline areas formed with the AC_{40}- and the ABC_{23}-tagged RNA polymerase, respectively. (*B*) The projection maps shown in *A* correspond to characteristic orientations of the RNA polymerase molecule, and define which face of a previously calculated three-dimensional molecular model (Schultz et al., 1993) interacts with the lipid film. For the sake of clarity, only the surface representation of an RNA polymerase monomer is shown. The position of the lipid film is indicated by circles and lines symbolizing the lipid molecule. The spatial location of the His_6-tagged subunits, as determined previously by immuno-electron microscopy at a resolution of ~4 nm (Klinger et al., 1996; Lanzendörfer et al., 1997), is labeled by a white spot. These representations show that in both crystal forms, the tagged subunit is in contact with the lipid layer.

(Schultz et al., 1990) and a specific metal-chelating interaction, thus allowing the comparison of the two methods independently of the biological system. The most striking observation is the remarkable reproducibility of the crystallization experiments when a specific interaction is used. In our hands, the experiments using charged lipids were poorly reproducible with the same enzyme preparation and varied considerably from one enzyme preparation to the other. This poor reproducibility is probably due to the dramatic influence of electrostatic charges within and around the incubation well and to small variations in protein purity. The specific interaction appears more robust in these respects, because electrostatic interactions were shown to be of minor importance in the crystallization process and because contaminants, such as a fivefold molar excess of streptavidin, had little influence on the protein-lipid interaction. The crystals obtained with the specific lipid were not better ordered than those formed on charged layers, indicating that the transfer mechanism, the structural preservation, or the homogeneity of the protein rather than the tethering to the lipid layer limits their use for high-resolution structural studies. Analysis of crystal defects reveals that the individual dimers may be severely tilted within the crystalline area (data not shown), thus suggesting that the transfer and staining protocols introduce at least part of the disorder. We hope that cryo-electron microscopy of frozen-hydrated crystals will sort out these various questions (Dubochet et al., 1988).

The crystals obtained with the specific lipid were not larger than those formed on charged lipids, but the distribution of the organized areas was distinct. In most instances, the crystals formed on charged lipids were contiguous to regions covered with isolated molecules. Crystals formed in the presence of the specific Ni-chelating lipids were segregated in oval-shaped domains. This behavior probably reflects a property of the lipid rather than the recruitment of all RNA polymerase molecules into crystals, because similar domains formed when the saturated lipid was used where the distance between isolated molecules excludes protein-protein interactions. Previous reports indicated that the properties of this family of lipids vary with time and that diluted lipid solutions lose their ability to promote crystallization (Barklis et al., 1997; Venien-Bryan, personal communication). Although no activity loss was observed with time, it is conceivable that part of the lipid molecules are degraded and form two distinct phases, only one of which would be able to bind the protein.

The kinetics of crystal growth were comparable to both specific and nonspecific lipids, which is consistent with the proposal that crystallization is mainly driven by protein-protein interactions. A major difference was the formation, after long incubation times, of multilayered structures that were not observed for yeast RNA polymerase I when charged lipids were used. Similar structures would appear in the case of epitaxial crystal growth from the 2-D crystals, as described for yeast RNA polymerase II on charged lipids (Darst et al., 1991b) and for streptavidin on specific lipids (Hemming et al., 1995), and thus would not be a specific event associated with functionalized lipids. However, the multilayered structures observed in the present work do not share all of the properties expected for an epitaxial process. Most importantly, the nth layers can be in variable register as compared to the $(n - 1)$th, and as a result no moiré pattern could be observed. It is possible, however, that because of the defects and large amount of twinning of the underlying crystal, the upper layer is not in register. In the case of the B subunit of cholera toxin, a helical growing mechanism was proposed to explain the formation of multilayer structures (Mosser and Brisson, 1991; and Mosser, unpublished observations). Platinum shadowing of His_6-tagged RNA polymerase I multilayers indicated that the multiple stacks do not obey a helical growth model (data not shown). As an alternative mechanism, 2-D crystals may detach from the interface and be randomly deposited on the carbon support used for electron microscopy. The adsorption onto the carbon foil needs then to be directional, because all crystals adopt the same orientation. Whatever the exact mechanism, the formation of multilayers requires protein-protein interactions, as evidenced by the high proportion of stacks compared to the protein-free surfaces and

by the observation that the upper layer rarely stretches out beyond the edges of the lower one.

Potential use of nonfluid lipid layers

The saturated lipids have a reduced fluidity compared to the unsaturated molecules and prevent crystallization of His_6-tagged RNA polymerase. As demonstrated for other systems (Darst et al., 1991a; Mosser and Brisson, 1991), the low fluidity of these lipids reduces the lateral mobility of the bound proteins and impairs their in-plane interactions. As a consequence, the saturated lipids allow us to bind and transfer protein complexes at concentrations in the 10^{-8} molar range, which then adopt a stochastic distribution ideal for structural studies of isolated particles. This is a considerable advantage as compared to fluid lipids, with which it is difficult to obtain a homogeneous distribution of particles, which tend to aggregate if they fail to crystallize. Such rigid supports represent a favorable alternative to carbon supports, the adsorption conditions of which are poorly understood. An important property is that maximally compressed lipid film prevents hydrophobic interactions of proteins with the support, which could denature the specimen. It is further possible to modulate the environment of the protein complex by adding charged headgroups in the lipid layer. Moreover, the biological activity of the lipid-bound enzyme can be tested, and the physiological significance of the observed structure can be validated by using large lipid monolayers formed on multicompartment troughs (Peters and Fromhertz, 1975).

A predicted property of the specific interaction of the enzyme with the lipid film is that all RNA polymerase molecules should have the same orientation relative to the lipid plane. As shown above, the His_6-tagged RNA polymerase molecules are specifically oriented in the 2-D crystals. An oriented adsorption is of highest interest for structural studies of isolated molecules, where individual molecular images are aligned in rotation and translation before being averaged. Averaging is possible only when all molecules are viewed along the same direction; therefore an additional step is necessary to partition the images into classes corresponding to different molecular views (Frank, 1996). The situation is even more complex when the molecular assembly can adopt various conformations or consists of a heterogeneous population. Thus by reducing the complexity of the data set, an oriented adsorption of the molecular complexes will help to partition the images according criteria other than orientation. Our experiments failed to demonstrate that the RNA polymerase molecules are oriented with respect to the lipid film. We attribute this observation to disorder introduced by the transfer, staining, and drying steps, which may modify the orientation of the RNA polymerase molecule. In this respect it is worth noting that the expected orientation is not favorable, because it corresponds to a situation where the longest dimension of the enzyme is perpendicular to the lipid plane. We expect that a larger number of molecules will be oriented when the hydrated specimen is preserved in a vitrified state (Dubochet et al., 1988).

We thank V. Mallouh for support in image processing and J. C. Homo for help with electron microscopes.

This work was supported by funds from the Institute National de la Santé et de la Recherche Médicale, the Centre National de la Recherche Scientifique, and the Centre Hospitalier Universitaire Régional and the Deutsche Forschungsgemeinschaft.

REFERENCES

Altenburger, J. M., L. Lebeau, C. Mioskowski, and D. Schirlin. 1992. Synthesis of new glycero lipids linked to hydroxamate derivatives designed for two-dimensional crystallisation of amino peptidase M. *Helv. Chim. Acta.* 75:2538–2544.

Avila-Sakar, A. J., T. L. Guan, T. Arad, M. F. Schmid, T. W. Loke, A. Yonath, J. Piefke, F. Franceschi, and W. Chiu. 1994. Electron cryomicroscopy of *Bacillus stearothermophilus* 50 S ribosomal subunits crystallized on phospholipid monolayers. *J. Mol. Biol.* 239:689–697.

Barklis, E., J. McDermott, S. Wilkens, E. Schabtach, M. F. Schmid, S. Fuller, S. Karanjia, Z. Love, R. Jones, Y. Rui, X. Zhao, and D. Thompson. 1997. Structural basis of membrane-bound retrovirus capsid proteins. *EMBO J.* 16:1199–1213.

Célia, H., L. Hoermann, P. Schultz, L. Lebeau, V. Mallouh, D. B. Wigley, J. C. Wang, C. Mioskowski, and P. Oudet. 1994. Three-dimensional model of *Escherichia coli* gyrase B subunit crystallized in two-dimensions on novobiocin-linked phospholipid films. *J. Mol. Biol.* 236: 618–628.

Célia, H., J. D. Jontes, M. Whittaker, and R. A. Milligan. 1996. Two-dimensional crystallization of brush border myosin I. *J. Struct. Biol.* 117:236–241.

Darst, S. A., M. Ahlers, P. H. Meller, E. W. Kubalec, R. Blankenburg, H. O. Ribi, H. Ringsdorf, and R. D. Kornberg. 1991a. Two-dimensional crystals of streptavidin on biotinylated lipid layers and their interactions with biotinylated macromolecules. *Biophys. J.* 59:387–396.

Darst, S. A., E. W. Kubalek, A. M. Edwards, and R. D. Kornberg. 1991b. Two-dimensional and epitaxial crystallization of a mutant form of yeast RNA polymerase II. *J. Mol. Biol.* 220:347–357.

Darst, S. A., E. W. Kubalec, and R. D. Kornberg. 1989. Three-dimensional structure of *Escherichia coli* RNA polymerase holoenzyme determined by electron crystallography. *Nature.* 340:730–732.

Dietrich, C., O. Boscheinen, K. D. Scharf, L. Schmitt, and R. Tempé. 1996. Functional immobilization of a DNA-binding protein at a membrane interface via histidine tag and synthetic chelator lipids. *Biochemistry.* 35:1100–1105.

Dietrich, C., L. Schmitt, and R. Tempé. 1995. Molecular organisation of histidine-tagged biomolecules at self-assembled lipid interfaces using a novel class of chelator lipids. *Proc. Natl. Acad. Sci. USA.* 92: 9014–9018.

Dubochet, J., M. Adrian, J.-J. Chang, J.-C. Homo, J. Lepault, A. W. McDowall, and P. Schultz. 1988. Cryo-electron microscopy of vitrified specimens. *Q. Rev. Biophys.* 21:129–228.

Edwards, A. M., S. A. Darst, S. A. Hemming, Y. Li, and R. D. Kornberg. 1994. Epitaxial growth of protein crystals on lipid layers. *Struct. Biol.* 1:195–197.

Ellis, M. J., H. Hebert, and M. Thelestam. 1997. *Staphylococcus aureus* alpha-toxin: characterization of protein/lipid interactions, 2D crystallization on lipid monolayers, and 3D structure. *J. Struct. Biol.* 118: 178–188.

Frank, J. 1996. Three-Dimensional Electron Microscopy of Macromolecular Assemblies. Academic Press, New York.

Frey, W., W. R. Schief, D. W. Pack, C.-T. Chen, A. Chilkoti, P. Stayton, V. Vogel, and F. H. Arnold. 1996. Two-dimensional protein crystallisation via metal-ion coordination by naturally occuring surface histidines. *Proc. Natl. Acad. Sci. USA.* 93:4937–4941.

Hemming, S. A., A. Bochkarev, S. A. Darst, R. D. Kornberg, P. Ala, D. S. C. Yang, and A. M. Edwards. 1995. The mechanism of protein crystal growth from lipid layers. *J. Mol. Biol.* 246:308–316.

Henderson, R., J. M. Baldwin, T. A. Ceska, F. Zemlin, E. Beckmann, and K. H. Downing. 1990. Model for the structure of bacteriorhodopsin based on high-resolution electron cryo-microscopy. *J. Mol. Biol.* 213: 899–929.

Huet, J., H. Phalente, G. Buttin, A. Sentenac, and P. Fromageot. 1982. Probing yeast RNA polymerases subunits with monospecific antibodies. *EMBO J.* 1:1193–1198.

Hochuli, E., H. Dobeli, and A. Schacher. 1987. New metal chelate adsorbent selective for proteins and peptides containing neighboring histidine residues. *J. Chromatogr.* 411:177–184.

Klinger, C., J. Huet, D. Song, G. Petersen, M. Riva, E. K. F. Bautz, A. Sentenac, P. Oudet, and P. Schultz. 1996. Localization of yeast RNA polymerase I core subunits by immuno-electron microscopy. *EMBO J.* 15:4643–4653.

Kubalek, E. W., S. F. J. Le Grice, and P. O. Brown. 1994. Two-dimensional crystallization of histidine-tagged, HIV-1 reverse transcriptase promoted by a novel nickel-chelating lipid. *J. Struct. Biol.* 113:117–123.

Kühlbrandt, W., D. N. Wang, and Y. Fujiyoshi. 1994. Atomic model of plant light-harvesting complex by electron crystallography. *Nature.* 367: 614–621.

Lanzendörfer, M., A. Smid, C. Klinger, P. Schultz, A. Sentenac, C. Carles, and M. Riva. 1997. A shared subunit belongs to the eukaryotic core RNA polymerase. *Genes Dev.* 11:1037–1047.

Lebeau, L., E. Regnier, P. Schultz, J. C. Wang, C. Mioskowski, and P. Oudet. 1990. Two-dimensional crystallisation of DNA gyrase B subunit on specifically designed lipid monolayers. *FEBS Lett.* 267:38–42.

Lebeau L., P. Schultz, H. Célia, P. Mesini, S. Nuss, C. Klinger, S. Olland, P. Oudet, and C. Mioskowski. 1996. Specifically designed lipid assemblies as tools for two-dimensional crystallization of soluble biological macromolecules. *In* Handbook of Nonmedical Applications of Liposomes, Vol. II. Y. Barenholz and D. D. Lasic, editors. CRC Press, Boca Raton, FL. 155–188.

Mosser, G., and A. Brisson. 1991. Conditions of two-dimensional crystallisation of cholera toxin B-subunit on lipid films containing ganglioside GM1. *J. Struct. Biol.* 106:191–198.

Pack, D. W., G. Chen, K. M. Maloney, C.-T. Chen, and F. H. Arnold. 1997. A metal-chelating lipid for 2-D protein crystallization via coordination of surface histidines. *J. Am. Chem. Soc.* 119:2479–2487.

Peters, J., and P. Fromhertz. 1975. Interaction of electrically charged lipid monolayers with malate dehydrogenase. *Biochim. Biophys. Acta.* 394: 111–119.

Porath, J., J. Carlson, I. Olsson, and G. Belfrage. 1975. Metal chelate affinity chromatography, a new approach to protein fractionation. *Nature.* 258:598–599.

Ribi, H. O., P. Reichard, and R. D. Kornberg. 1987. Two-dimensional crystals of enzyme effector complexes: ribonucleotide reductase at 18 Å resolution. *Biochemistry.* 26:7974–7979.

Saxton, W. O. 1980. Digital processing of electron images: a survey of motivations and methods. *In* Proceedings of the 7th European Congress on Electron Microscopy, The Hague, Vol. 2. 682–689.

Schmitt, L., C. Dietrich, and R. Tempé. 1994. Synthesis and characterization of chelator-lipids for reverse immobilization of engineered proteins at self assembled lipid interfaces. *J. Am. Chem. Soc.* 116:8485–8491.

Schmutz, M., and A. Brisson. 1996. Analysis of carbon film planarity by reflection light microscopy. *Ultramicroscopy.* 63:263–272.

Schultz, P., H. Célia, M. Riva, P. Colin, S. A. Darst, R. D. Kornberg, A. Sentenac, and P. Oudet. 1990. Two-dimensional crystals of yeast RNA polymerase A. *J. Mol. Biol.* 216:353–362.

Schultz, P., H. Célia, M. Riva, A. Sentenac, and P. Oudet. 1993. Three-dimensional model of yeast RNA polymerase I determined by electron microscopy of two-dimensional crystals. *EMBO J.* 12:2601–2607.

Unwin, N. 1993. Nicotinic acetylcholine receptor at 9 Å resolution. *J. Mol. Biol.* 229:1101–1124.

Uzgiris, E. E., and R. D. Kornberg. 1983. Two-dimensional crystallization technique for imaging macromolecules, with application to antigen-antibody-complement complexes. *Nature.* 301:125–127.

Van Heel, M., and J. Frank. 1981. Use of multivariate statistics in analysing the images of biological macromolecules. *Ultramicroscopy.* 6:187–194.

Van Heel, M., and W. Keegstra. 1981. IMAGIC: a fast, flexible and friendly image analysis software system. *Ultramicroscopy.* 7:113–130.